Functional group quantification of polymer nanomembranes with soft x-rays

Daniel F. Sunday, Edwin P. Chan, Sara V. Orski, Ryan C. Nieuwendaal, and Christopher M. Stafford

Phys. Rev. Materials **2**, 032601 — Published 15 March 2018

DOI: 10.1103/PhysRevMaterials.2.032601

Functional Group Quantification of Polymer Nanomembranes with Soft X-rays

Daniel F. Sunday, Edwin P. Chan, Sara V. Orski, Ryan C. Nieuwendaal, and Christopher M. Stafford*
Materials Science and Engineering Division, National Institute of Standards and Technology, Gaithersburg, MD 20899, USA
(Dated: March 1, 2018)

Polyamide nanomembranes are at the heart of water desalination, a process which plays a critical role in clean water production. Improving their efficiency requires a better understanding of the relationship between chemistry, network structure and performance but few techniques afford compositional information in ultrathin films (<100 nm). Here we leverage resonant soft X-ray reflectivity, a measurement that is sensitive to the specific chemical bonds in organic materials, to quantify functional group concentration in these polyamides. We first employ reference materials to establish quantitative relationships between changes in the optical constants and functional group density, and then use the results to evaluate the functional group concentrations of polyamide nanomembranes. We demonstrate that the difference in the amide carbonyl and carboxylic acid group concentrations can be used to calculate the crosslink density, which is shown to vary significantly across three different polyamide chemistries. A clear relationship is established between the functional group density and the permselectivity (α), indicating that more densely crosslinked materials result in higher α of the nanomembranes. Finally, measurements on a polyamide/poly(acrylic acid) bilayer demonstrate the ability of this approach to quantify depth-dependent functional group concentrations in thin films.

PACS numbers: Valid PACS appear here

Current desalination membranes are hierarchically structured materials consisting of an ultrathin crosslinked polyamide permselective layer on a porous support. This polyamide permselective layer is critical to the separation of ions (i.e. salt) from water and is produced by reacting a triacid chloride (TMC) with an aromatic diamine, either via interfacial polymerization or the recently developed molecular layer-by-layer (mLbL) method [1, 2]. The resulting polyamide contains several defining chemical moieties: amide groups (NHCO) that represent crosslink junctions, and free carboxylic acids (COOH) and amines (NH_2) (Fig. 1). These unreacted COOH and NH_2 groups are viewed as defects in the network structure; however, some amount of free COOH is desirable to enhance solubility of water in the membrane as prior studies suggest that the desalination performance is determined by concentration of these chemical moieties [3]. Swelling measurements show that the polyamides produced using diethylene diamine swells almost 1.4× more than a membrane synthesized with aromatic diamines [4]. This difference in the swelling behavior implies a difference in the crosslinking density, which should correspond to differences in [NHCO].

Despite the widespread use of these materials [5], there remains a knowledge gap in the relationships between membrane chemistry, network structure and the extrinsic membrane properties that define membrane performance. Characterizing the chemistry of a bulk polyamide sample is straightforward but characterizing these chemical moieties for ultrathin polyamide films is nontrivial as they are ≈100 nm thick. Additionally, the degree of compositional homogeneity in these films is unclear, and it would be significantly beneficial to quantify the potential depth-dependent heterogeneity [6, 7].

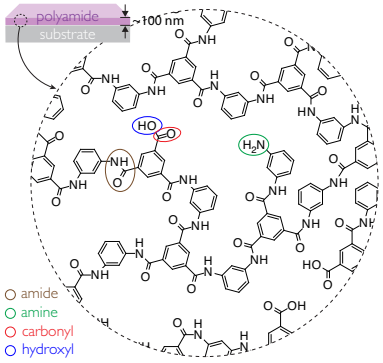

FIG. 1: The four functional groups of poly(*m*-phenylene diamine trisamide) (P*m*PDTA).

There is a critical need for quantitative depth profiling of the functional group densities for ultrathin polymeric materials, but the current approaches that address this metrology gap have limited depth resolution, require layer-by-layer analysis, or are often destructive (e.g., near edge X-ray absorption for fine structure (NEXAFS) [8, 9], X-ray photoelectron spectroscopy (XPS) [10, 11], secondary ion mass spectrometry (SIMS) [12]). Alternatively, X-ray reflectivity is non-destructive and is capable of characterizing the depth profile of the refractive index, which for hard X-rays corresponds to the electron density profile [13–15]. In the soft X-ray region (≈ 100 eV - 3000 eV), there are a significant number of atomic absorption edges where the refractive index of a material changes based on the bonding state, atomic concentration and the proximity of the beam energy to the absorption edge, providing a unique sensitivity to the

*Electronic address: daniel.sunday@nist.gov

chemical composition of the film. Studies utilizing this sensitivity have focused on determining phase distribution and interface behavior (for soft materials) [16–21] or the atomic composition depth profile (for hard materials) [22–25]. In this work, we apply resonant soft X-ray reflectivity (RSoXR) to determine the concentration of specific functional groups within three representative types of polyamide nanomembranes used in water desalination, as well as provide a quantitative evaluation of their network structure in order to relate these results to their separation performance.

Our approach to quantifying the functional group concentration of polyamides using RSoXR is a two-part process [26]. We first generate calibration curves for the specific functional groups of interests (related to the oscillator strength and functional group density), which are CO, OH, NHCO and NH_2, by conducting RSoXR measurements on polymers that we refer to as reference materials as they have known concentrations of the specific chemical moiety. Poly(acrylic acid) (PAA), poly(vinyl benzoic acid) PVBA, and poly(styrene-co-vinyl benzoic acid) having a mole fraction of 0.44 VBA (PVBA50), with known [COOH] are used to generate the calibrations for CO and OH functional groups. Several compositions of poly(styrene-co-*n*-phenylacrylamide) (PPHAM), with known [NHCO], are used to generate the calibrations for NHCO and NH_2 functional groups. We then conduct RSoXR measurements on the three polyamides to quantify their functional group concentrations by using the calibration curves obtained from the reference materials.

The underlying physics of using RSoXR for quantifying functional group concentration is that the optical constants of a material (δ and β, which are related to the complex refractive index, $n = 1 - \delta - i\beta$) is a function of the complex atomic scattering factor ($f(E)$). Quantitative relationships of δ and β with E determine the oscillator strength (g_s) and functional group density (ρ_s) for a given bond since they are defined by the functions,

$$n = 1 - \delta + i\beta = 1 - \frac{\lambda^2 r_e}{2\pi} \sum_s \rho_s f_s(E), \tag{1}$$

$$f_s(E) = \frac{g_s E^2}{E^2 - {E_s}^2 + i\gamma E}, \tag{2}$$

where λ is the X-ray wavelength, r_e is the classic electron radius. The additive nature of $f_s(E)$ to n allows the contributions from resonant and non-resonant components in a material to be evaluated separately. $f_s(E)$ for a given bond is calculated by modeling the behavior of the bond as a harmonic oscillator (Eq. (2)), where E_s is the energy at the absorption peak and γ is the width of the transition. We note that δ and β at a single energy near an absorption edge cannot be directly used to determine ρ_s because the overall electron density of the film also impacts the absolute value of the optical constants. Instead, δ and β at the absorption edge are rescaled relative to a non-resonant energy. Specifically, we use $\Delta\delta$ and $\Delta\beta$ relative to this non-resonant energy rather than δ and β in order to isolate the resonant contributions and quantify the ρ_s irrespective of the film's mass density,

$$\Delta\delta = \delta_{nr} - \delta_r, \tag{3}$$

$$\Delta\beta = \beta_r - \beta_{nr}, \tag{4}$$

where the nr subscript indicates a non-resonant reference energy. The conventions are defined such that $\Delta\delta$ and $\Delta\beta$ are generally positive.

Representative RSoXR curves for PSVBA50 for incident energies $E = 500$ eV to $E = 540$ eV are shown in Fig. 2a. At 500 eV, E is far enough from the absorption edge to be considered non-resonant. As E increases, the critical edge of the film begins to shift to lower scattering vector (Q) (Fig. 2a), corresponding to a decrease in electron density, i.e., δ (Fig. 2b). A minimum in β is observed at 531.75 eV, as E increases β increases rapidly as the peak in the 1s$\rightarrow \pi*$ transition for CO is approached (532.25 eV) (Fig. 2c). The 1s$\rightarrow \sigma*$ transition for OH occurs at higher energies, with the δ minima and β maxima occurring at 534 eV and 534.5 eV, respectively. The optical constants for each film were evaluated by fitting the RSoXR curves to a three-layer reflectivity model, which included the silicon substrate, a thin layer of silicon oxide and the polymer. The optical constants for the substrate and oxide were estimated based on reference values [27] whereas the optical constants, thickness and roughness of the polymer layer were allowed to vary.

Fits to $\Delta\delta$ and $\Delta\beta$ for all three references are shown in Fig. 2e and Fig. 2f, respectively. Details of the fitting procedure is provided in the Supplementary Information section. The PVBA and PAA films are qualitatively similar to the PSVBA50 curve, and the magnitude of $\Delta\delta$ and $\Delta\beta$ scale with [COOH]. Fig. 2g shows the calibration curves ($\rho_s g_s$ vs. ρ_s) obtained from the RSoXR fitting routine using the PAA, PVBA and PSVBA50 references with known [COOH]. These curves provide a means for evaluating [CO] and [OH] of the polyamides.

Besides constructing calibration curves for CO and OH, we attempted to construct calibrations for NHCO and NH_2 via RoSXR measurements at the nitrogen edge using the same experimental and fitting approaches. The results of these measurements are shown in the Supplemental Information (Fig. S5). While there are clearly qualitative differences between the aromatic and non-aromatic films, the individual transitions are more difficult to distinguish in this region. Thus quantifying the functional group concentration is not possible without explicitly modeling the transitions [28–30].

Next, model polyamide films, identical in chemistry to commercial desalination membranes, were prepared via mLbL by reacting TMC and one of three diamines (diethylene diamine (DD), *p*-phenylene diamine (*p*PD) and *m*-phenylene diamine (*m*PD)) to produce poly(diethylene diamine trisamide) (PDDTA), poly(*p*-phenylene diamine trisamide) (P*p*PDTA) and poly(*m*-phenylene diamine trisamide) P*m*PDTA, respectively.

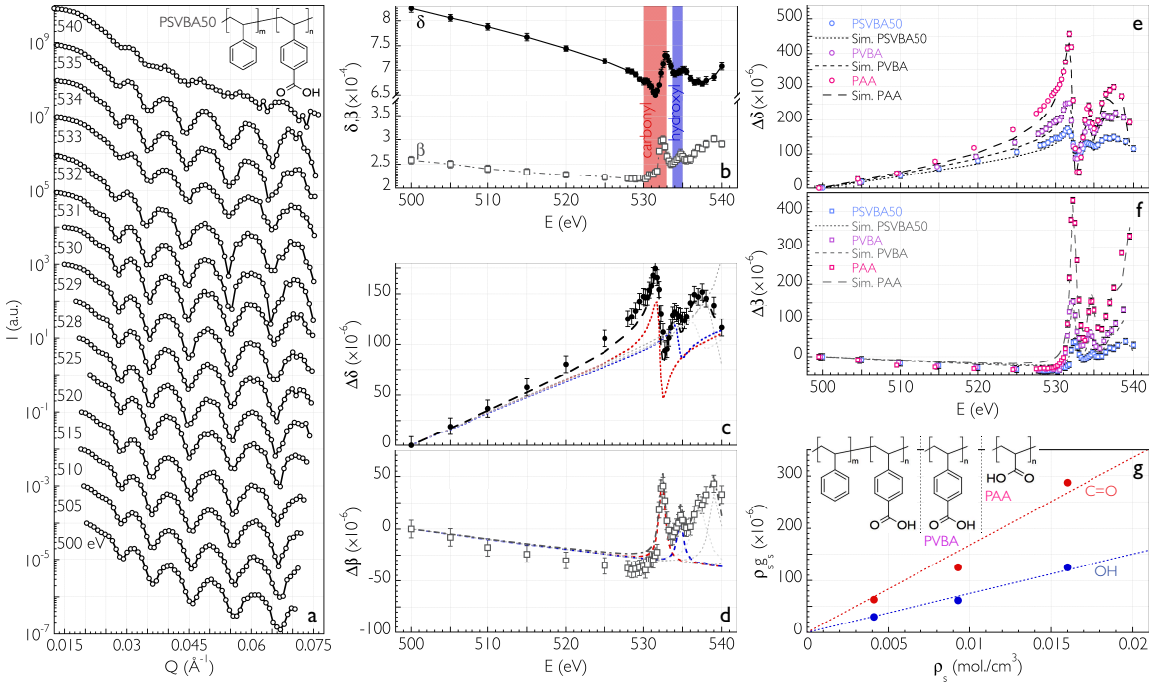

FIG. 2: a) RSoXR curves for PSVBA50 from $E = 500$ eV to $E = 540$ eV. b) δ and β extracted from the curves at each E. The red background highlights the region sensitive to the CO bond and the blue background highlights the region sensitive to the OH bond. c) $\Delta\delta$ and d) $\Delta\beta$ relative to 500 eV (calculated with Eq. (1) and Eq. (2)) for the experimental data (error bars represent 95% confidence intervals using a directed evolution Monte Carlo Markov Chain algorithm (DREAM)) [31] and simulated fits for the individual transitions (dashed line, CO red, OH blue, additional transitions grey). The black line is the sum contributions from the individual bonds calculated with Eq. (1). e) $\Delta\delta$ and f) $\Delta\beta$ for PAA, PVBA and PSVBA50 as a function of E. Experimental data is shown by the open symbols, simulated fits are shown with the dashed line. g) $g_s\rho_s$ vs. ρ_s for the references along with the chemical formulas. Dashed lines are linear fits to the data.

Details of mLbL are provided in the Supplemental Information section.

$\Delta\delta$ and $\Delta\beta$ curves for the three polyamides illustrate a qualitative view of the differences in functional group densities (Fig. 3(a,c,e) and Fig. 3(b,d,f)). Specifically, PmPDTA and PpPDTA have similar $\Delta\delta$ at 531.75 (CO 1s$\rightarrow \pi*$), which indicates a similar concentration of CO groups, whereas PDDTA has a higher density of CO groups, as indicated by the larger $\Delta\delta$ at that energy. Similar trends in $\Delta\beta$ between the three materials are observed at 532.25 eV. The magnitude of the shifts for $\Delta\delta$ and $\Delta\beta$ near the OH transition are smaller than any of the reference materials, indicating lower [COOH]. After fitting these curves using the same approach for the reference materials, $\rho_s g_s$ was determined and referenced to the calibration curve as shown in Fig. 3g. [CO] and [OH] of the polyamides are shown in Table I.

ρ_s at the oxygen edge can provide insight into the structure-performance relationships for water desalination membranes. The ratio between [OH] and [CO] for each polyamide can be used to determine the average crosslink density of the material, and we use these ratios to construct representative network structures for PDDTA, PpPDTA and PmPDTA (Fig. 4a). These structures illustrate that the three different chemistries lead to changes in pore size, PDDTA has the largest average pore, formed between crosslinked junctions, whereas PmPDTA has the smallest pore and PpPDTA is intermediate to these two materials. It also shows agreement with the trends observed via swelling measurements, where the swelling is inversely proportional to the crosslink density seen here. In all three polyamides, the crosslink density is approximately two times lower than the reported values of similar polyamide films measured via vapor swelling [4]. We attribute the slight discrepancies to either the thickness dependent crosslink density or the presence of network defects. Chan *et al.* have recently reported the thickness-dependent crosslink density of PmPDTA thin films to show that the crosslink density increases with increasing film thickness up to $\approx$ 72 nm [7]. Network defects such as dangling bonds will affect the swelling behavior, and thus the pore size, of a polymer network. Traditional network swelling models will account for these defects by underestimating the crosslink density. As an upper limit estimation of the crosslink density, we assumed that the polyamides presented in Fig. 4a are defect-free. The discrepancy between the current study and the prior one suggests that network defects consisting of NH_2 are present in all three polyamides. The quantification of the NHCO and NH_2 would provide a complete picture of the network structure by accounting for these defects. Given current limi-

TABLE I: Fits for CO and OH bonds for the polyamide films.

Sample	$\rho_s g_s$ CO ($\times 10^4$)	[CO]* mmol/cm^3	$\rho_s g_s$ OH ($\times 10^4$)	[OH]* mmol/cm^3	[CO]/[OH]
PDDTA	1.75	10.2 ± 0.8	0.156	2.1 ± 0.5	4.8
PpPDTA	1.5	8.7 ± 0.7	0.06	0.8 ± 0.4	10.8
PmPDTA	1.47	8.6 ± 0.7	0.037	0.5 ± 0.3	17.2

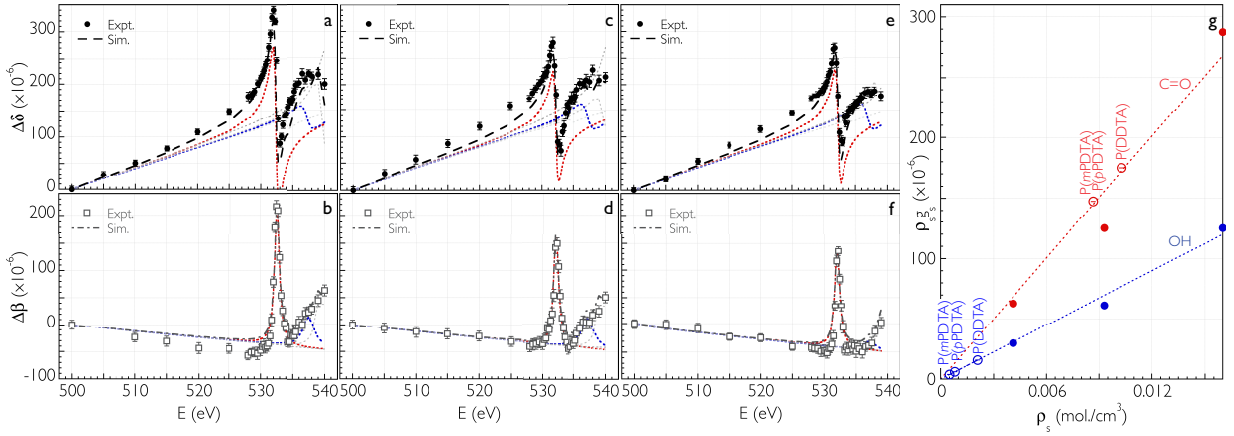

FIG. 3: Changes in $\Delta\delta$ and $\Delta\beta$ of the polyamides. a) $\Delta\delta$ and b) $\Delta\beta$ for PDDTA. (c) $\Delta\delta$ and d) $\Delta\beta$ for PpPDTA. e) $\Delta\delta$ and f) $\Delta\beta$ for PmPDTA. g) Applying the calibration curves obtained from the references to determine [CO] and [OH] of the polyamides (open symbols), solid dots indicate reference samples, dashed line is the reference curve.

tations, this will be the focus of future works.

We use these results to improve our understanding of the factors impacting membrane performance by comparing the functional group concentrations with the permselectivity (α), which is a dimensionless ratio between the water permeability and sodium chloride permeability. Fig. 4b is a plot of α from literature values, as a function of [OH] and [CO] of the polyamides [32]. The plot suggests that α is strongly dependent on [OH] but has a weak dependence with [CO]. The relationship between α and [CO] is not surprising given that monomer dimensions for the three polyamides are quite similar, which implies that [CO] would be similar as well. However, the strong correlation between α and [OH] is an interesting one because prior attempts to develop such a correlation has been limited to oxygen-to-nitrogen atomic composition of the polyamide surface via XPS as opposed to specific functional groups [1, 4]. We can gain further insight into these results by expressing Fig. 4b as a plot of α versus [OH]/[CO], which serves as a measure of the number of OH groups per monomer unit (Fig. 4c). From this figure, we find that the selectivity increases with decreasing [OH]/[CO], which is consistent with the molecular picture of smaller pores enhancing sieving ability as illustrated schematically in Fig. 4a. The water permeability, which can be viewed as the inverse of the selectivity based on performance tradeoff relationship [33], increases with [OH]/[CO], which again is consistent with the notion that larger pores lead to higher water permeation.

To demonstrate the ability of this approach to clearly differentiate between layers with different functional group densities, we prepared a bilayer consisting of PmPDTA layer on top of a PAA film. The RSoXR curves are shown in Fig. S6. At 500 eV, the modulations in the fringes indicates the presence of the bilayer structure, but as the energy is increased towards 530 eV the magnitude of the modulation increases, driven by the diverging change in optical constants for the two layers. **These curves were fitted with an additional PAA layer to the reflectivity model. This four layer model consists of the silicon substrate, a thin layer of silicon oxide, the PAA and the PmPDTA.** $\Delta\delta$ and $\Delta\beta$ for both layers are shown as a function of energy in Fig. 5a and Fig. 5b, respectively, along with the simulated fits used to quantify the functional group density. [CO] and [OH] as a function of depth is shown in Fig. 5c. The width of the interface layer between the PAA and PmPDTA is considerably **thinner** than the individual layers, and demonstrates the feasibility of this approach for the quantitative depth profiling of the functional group density in thin films.

In conclusion, we have developed a new measurement approach that utilizes soft X-ray reflectivity to characterize the functional group concentrations in thin films. Using calibration samples with known functional group densities, the relationship between the change in the optical constants and functional group concentration was determined. This calibration curve was then used to quantify the CO and OH group concentration in a series of polyamide nanomembranes with different

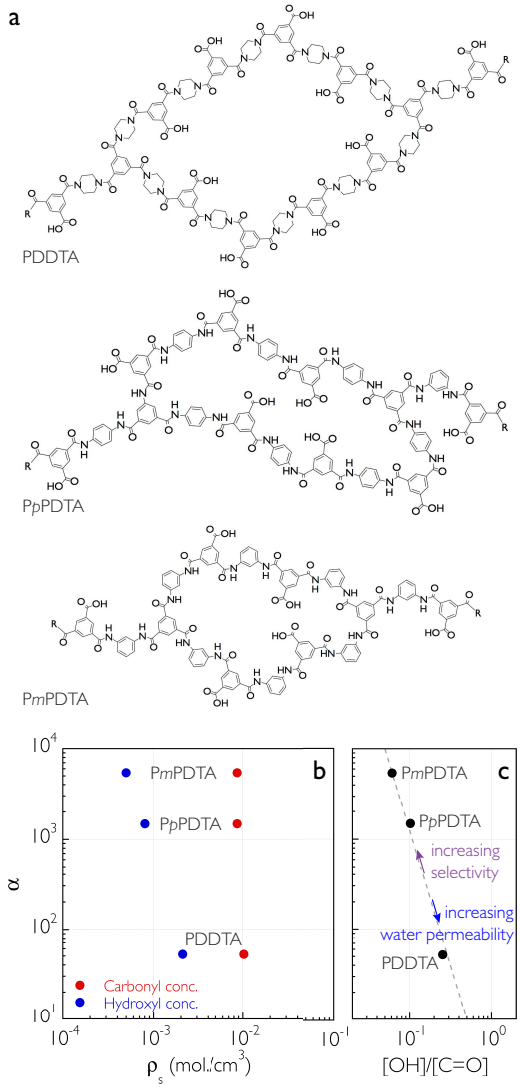

FIG. 4: a) Predicted aromatic polyamide network structures based on the functional group concentrations. b) Permselectivity, α, vs. functional group concentration for the three polyamides. c) α vs. [OH]/[CO] for the three polyamides. The dashed line represents the best fit to the data points.

chemistries. From this result direct correlations between the densities of these functional groups, and therefore the crosslinking densities with the intrinsic membrane parameters were observed. These results suggest that the optimum membrane system would have both dense crosslinks and a high concentration of COOH. In addition to determining the functional group concentration in these films measurements on a PAA, P*m*PDTA bilayer demonstrated the ability of this approach to depth profile the concentration of functional groups in a film. While the demonstration of this technique focused on oxygen containing functional groups, this approach is generalizable to a wide range of different chemistries. Finally, this technique could be adapted to the transmission-based scattering measurements to interrogate problems that aren't well suited for reflectivity measurements.

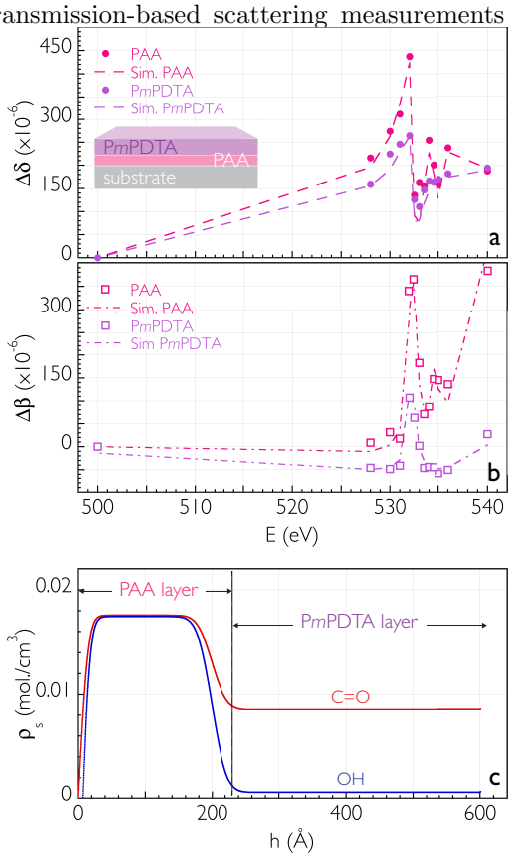

FIG. 5: a) $\Delta\delta$ for the PAA layer (experimental, simulated) and P*m*PDTA layer (experimental, simulated). b) $\Delta\beta$ for the PAA layer (experimental, simulated) and P*m*PDTA layer (experimental, simulated). c) Concentration profile of the CO and OH groups in the film.

Acknowledgments

The Advanced Light Source is supported by the Director, Office of Science, Office of Basic Energy Sciences, of the U.S. Department of Energy under Contract No. DE-AC02-05CH11231. We thank Eric Gullikson for assistance at BL. 6.3.2. We gratefully acknowledge Chris Soles for helpful discussions. This work is a contribution of NIST, an agency of the U.S. Government, and not subject to U.S. copyright.

[1] P. M. Johnson, J. Yoon, J. Y. Kelly, J. A. Howarter, and C. M. Stafford, Journal of Polymer Science Part B: Polymer Physics **50**, 168 (2012), ISSN 08876266, URL

http://doi.wiley.com/10.1002/polb.23002.

[2] E. P. Chan, J.-H. Lee, J. Y. Chung, and C. M. Stafford, Review of Scientific Instruments **83**, 114102 (2012).

[3] F. Foglia, S. Karan, M. Nania, Z. Jiang, A. E. Porter, R. Barker, A. G. Livingston, and J. T. Cabral, Adv. Funct. Mater. **27**, n/a (2017), ISSN 1616-3028, URL http://onlinelibrary.wiley.com/doi/10.1002/adfm.201701738/abstract.

[4] E. P. Chan, A. P. Young, J.-H. Lee, and C. M. Stafford, Journal of Polymer Science Part B: Polymer Physics **51**, 1647 (2013), URL http://onlinelibrary.wiley.com/doi/10.1002/polb.23380/full.

[5] J. R. Werber, C. O. Osuji, and M. Elimelech, Nature Reviews Materials **1**, 16018 (2016), URL http://dx.doi.org/10.1038/natrevmats.2016.18.

[6] F. Pacheco, R. Sougrat, M. Reinhard, J. O. Leckie, and I. Pinnau, Journal of Membrane Science **501**, 33 (2016), ISSN 03767388, URL http://linkinghub.elsevier.com/retrieve/pii/S037673881530291X.

[7] E. P. Chan and S. C. Lee, Journal of Polymer Science Part B: Polymer Physics **55**, 412 (2017), ISSN 08876266, URL http://doi.wiley.com/10.1002/polb.24285.

[8] H. Ade and A. P. Hitchcock, Polymer **49**, 643 (2008), ISSN 00323861, URL http://linkinghub.elsevier.com/retrieve/pii/S0032386107010270.

[9] S. Krishnan, M. Y. Paik, C. K. Ober, E. Martinelli, G. Galli, K. E. Sohn, E. J. Kramer, and D. A. Fischer, Macromolecules **43**, 4733 (2010), ISSN 0024-9297, 1520-5835, URL http://pubs.acs.org/doi/abs/10.1021/ma902866x.

[10] J. F. Watts and J. Wolstenholme, *An Introduction to Surface Analysis by XPS and AES* (Wiley and Sons, Chichester, United Kingdom, 2003).

[11] D. Briggs, *Surface Analysis of Polymers by XPS and Static SIMS* (Cambridge University Press, Cambridge, United Kingdom, 1998).

[12] P. Williams, Annual Review of Materials Science **15**, 517 (1985), URL http://www.annualreviews.org/doi/pdf/10.1146/annurev.ms.15.080185.002505.

[13] T. P. Russell, Physica B: Condensed Matter **221**, 267 (1996), URL http://www.sciencedirect.com/science/article/pii/092145269500937X.

[14] E. K. Lin, C. L. Soles, D. L. Goldfarb, B. C. Trinque, S. D. Burns, R. L. Jones, Joseph L. Lenhart, M. Angelopoulos, C. G. Willson, S. K. Satija, et al., Science **297**, 372 (2002), ISSN 0036-8075, 1095-9203, URL http://www.sciencemag.org/content/297/5580/372.

[15] V. M. Prabhu, S. Kang, D. L. VanderHart, S. K. Satija, E. K. Lin, and W.-l. Wu, Advanced Materials **23**, 388 (2011), ISSN 09359648, URL http://doi.wiley.com/10.1002/adma.201001762.

[16] H. Ade, C. Wang, A. Garcia, H. Yan, K. E. Sohn, A. Hexemer, G. C. Bazan, T.-Q. Nguyen, and E. J. Kramer, Journal of Polymer Science Part B: Polymer Physics **47**, 1291 (2009), ISSN 08876266, 10990488, URL http://doi.wiley.com/10.1002/polb.21730.

[17] D. F. Sunday, M. R. Hammond, C. Wang, W.-l. Wu, D. M. Delongchamp, M. Tjio, J. Y. Cheng, R. J. Kline, and J. W. Pitera, ACS Nano **8**, 8426 (2014), ISSN 1936-0851, 1936-086X, URL http://pubs.acs.org/doi/abs/10.1021/nn5029289.

[18] T. Araki, H. Ade, J. M. Stubbs, D. C. Sundberg, G. E. Mitchell, J. B. Kortright, and A. L. D. Kilcoyne, Applied Physics Letters **89**, 124106 (2006), ISSN 00036951, URL http://link.aip.org/link/APPLAB/v89/i12/p124106/s1&Agg=doi.

[19] C. Wang, T. Araki, and H. Ade, Applied Physics Letters **87**, 214109 (2005), ISSN 00036951, URL http://link.aip.org/link/APPLAB/v87/i21/p214109/s1&Agg=doi.

[20] C. Wang, T. Araki, B. Watts, S. Harton, T. Koga, S. Basu, and H. Ade, Journal of Vacuum Science & Technology A: Vacuum, Surfaces, and Films **25**, 575 (2007), ISSN 07342101, URL http://link.aip.org/link/JVTAD6/v25/i3/p575/s1&Agg=doi.

[21] D. F. Sunday, M. J. Maher, S. Tein, M. C. Carlson, C. J. Ellison, C. G. Willson, and R. J. Kline, ACS Macro Letters pp. 1306–1311 (2016), ISSN 2161-1653, 2161-1653, URL http://pubs.acs.org/doi/abs/10.1021/acsmacrolett.6b00684.

[22] M. Nayak and G. S. Lodha, Journal of Applied Crystallography **46**, 1569 (2013), ISSN 0021-8898, URL http://scripts.iucr.org/cgi-bin/paper?S0021889813022905.

[23] M. Nayak, P. C. Pradhan, and G. S. Lodha, Scientific Reports **5**, 8618 (2015), ISSN 2045-2322, URL http://www.nature.com/doifinder/10.1038/srep08618.

[24] S. Macke, A. Radi, J. E. Hamann-Borrero, M. Bluschke, S. Brck, E. Goering, R. Sutarto, F. He, G. Cristiani, M. Wu, et al., Adv. Mater. pp. n/a–n/a (2014), ISSN 1521-4095, URL http://onlinelibrary.wiley.com/doi/10.1002/adma.201402028/abstract.

[25] C. Park and P. A. Fenter, Journal of Applied Crystallography **40**, 290 (2007), ISSN 0021-8898, URL http://scripts.iucr.org/cgi-bin/paper?S0021889806053131.

[26] *Certain instruments and materials are identified in this paper to adequately specify the experimental details. Such iden- tification does not imply recommendation by the National Institute of Standards and Technology; nor does it imply that the materials are necessarily the best available for the purpose.*

[27] B. L. Henke, E. M. Gullikson, and J. C. Davis, Atomic Data and Nuclear Data Tables **54**, 181 (1993).

[28] S. N. Patel, G. M. Su, C. Luo, M. Wang, L. A. Perez, D. A. Fischer, D. Prendergast, G. C. Bazan, A. J. Heeger, M. L. Chabinyc, et al., Macromolecules **48**, 6606 (2015), ISSN 0024-9297, URL http://dx.doi.org/10.1021/acs.macromol.5b01647.

[29] R. Capelli, N. Mahne, K. Koshmak, A. Giglia, B. P. Doyle, S. Mukherjee, S. Nannarone, and L. Pasquali, The Journal of Chemical Physics **145**, 024201 (2016), ISSN 0021-9606, URL http://aip.scitation.org/doi/full/10.1063/1.4956452.

[30] L. Pasquali, S. Mukherjee, F. Terzi, A. Giglia, N. Mahne, K. Koshmak, V. Esaulov, C. Toccafondi, M. Canepa, and S. Nannarone, Phys. Rev. B **89**, 045401 (2014), URL https://link.aps.org/doi/10.1103/PhysRevB.89.045401.

[31] J. A. Vrugt and C. J. F. Ter Braak, Hydrol. Earth Syst. Sci. **15**, 3701 (2011), ISSN 1607-7938, URL https://www.hydrol-earth-syst-sci.net/15/3701/2011/.

[32] W. Choi, J.-E. Gu, S.-H. Park, S. Kim, J. Bang, K.-Y. Baek, B. Park, J. S. Lee, E. P. Chan, and J.-H. Lee, ACS Nano **9**, 345 (2015), ISSN 1936-0851, 1936-086X, URL http://pubs.acs.org/doi/abs/10.1021/nn505318v.

[33] G. M. Geise, H. B. Park, A. C. Sagle, B. D. Freeman, and J. E. McGrath, Journal of Membrane Science **369**, 130 (2011), ISSN 03767388, URL http://linkinghub.

elsevier.com/retrieve/pii/S0376738810009233.